Liquid Crystals
Publication details, including instructions for authors and subscription information:
http://www.informaworld.com/smpp/title~content=t713926090

Neutron scattering experiments on magnetically aligned liquid crystalline DNA fragment solutions

Leonore C. A. Groot[a]; Maxim E. Kuil[a]; Jaap C. Leyte[a]; Johan R. C. Van Der Maarel[a]; Richard K. Heenan[b]; Steve M. King[b]; Gerard Jannink[c]
[a] Department of Physical and Macromolecular Chemistry, University of Leiden, Gorlaeus Laboratories, Leiden, The Netherlands [b] Rutherford Appleton Laboratory, ISIS Facility, Oxon, England [c] Laboratoire Léon Brillouin, C. E. Saclay, Gif-sur-Yvette Cedex, France

To cite this Article Groot, Leonore C. A. , Kuil, Maxim E. , Leyte, Jaap C. , Van Der Maarel, Johan R. C. , Heenan, Richard K. , King, Steve M. and Jannink, Gerard(1994) 'Neutron scattering experiments on magnetically aligned liquid crystalline DNA fragment solutions', Liquid Crystals, 17: 2, 263 — 276
To link to this Article: DOI: 10.1080/02678299408036565
URL: http://dx.doi.org/10.1080/02678299408036565

LIQUID CRYSTALS, 1994, VOL. 17, NO. 2, 263–276

Neutron scattering experiments on magnetically aligned liquid crystalline DNA fragment solutions

by LEONORE C. A. GROOT, MAXIM E. KUIL, JAAP C. LEYTE and JOHAN R. C. VAN DER MAAREL*

University of Leiden, Gorlaeus Laboratories, Department of Physical and Macromolecular Chemistry, P.O. Box 9502, 2300 RA Leiden, The Netherlands

RICHARD K. HEENAN and STEVE M. KING

Rutherford Appleton Laboratory, ISIS Facility, Chilton, Didcot, Oxon, OX11 0QX, England

and GERARD JANNINK

Laboratoire Léon Brillouin†, C. E. Saclay, 91191 Gif-sur-Yvette Cedex, France

(*Received 27 October 1993; accepted 28 January 1994*)

Small angle neutron scattering experiments have been performed on liquid crystalline 163 basepair NaDNA fragments in aqueous solution in the concentration range 190–285 mg ml^{-1}. To induce a macroscopic alignment, a magnetic field was applied either parallel ($B_{\parallel}$ configuration) or perpendicular ($B_{\perp}$ configuration) to the incoming neutron beam. The isotropic scattering pattern in the $B_{\parallel}$ configuration and the anisotropic scattering in the $B_{\perp}$ configuration agree with the cholesteric structure of the liquid crystalline solutions. From the anisotropic scattering in the $B_{\perp}$ configuration, information on the orientation ordering can be derived. For this purpose, the experimental data are compared to the form function of a uniform rod including a gaussian orientation distribution. The standard deviation of this distribution is approximately 20° for all concentrations investigated here.

1. Introduction

Aqueous solutions of rod-like persistence length DNA fragments (500 Å) form liquid crystals above a certain concentration. This transition concentration depends on the low molecular weight salt concentration, the temperature [1] and presumably the origin of the DNA fragments [2]. These solutions undergo a series of phase transitions from the isotropic phase, via the cholesteric phase, and eventually to a hexagonal structure [1, 3–5].

Under the present conditions, the liquid crystalline solutions are cholesteric. The average local orientation of the molecules is defined by the director. In a cholesteric liquid crystal, the director is perpendicular to and rotates about the cholesteric axis throughout the sample. Accordingly, a helix structure appears with a macroscopic pitch of the order of 2×10^{-6} m [1, 6]. In the present contribution it is convenient to introduce the plane perpendicular to the cholesteric axis. This will be referred to as the director

* Author for correspondence.
† Laboratoire commun CEA-CNRS.

0267–8292/94 $10·00

plane, in which the director rotates. These solutions show optical birefringence [7] and NMR line-splittings are observed [2, 8, 9]. Brandes *et al.* [9], performed deuterium NMR experiments to investigate structural and dynamical aspects of the DNA molecules in the liquid crystalline state. They observed that the apparent amplitude of the base tilt motion was about 37°. However, regarding the origin of this relatively large amplitude, they could not distinguish between fluctuations in the orientations of the DNA molecules or base librations.

Solution structures can be investigated, for example, using small angle neutron (SANS) or X-ray (SAXS) scattering. The former method has the advantage that the partial structure functions can be obtained separately. This has been shown experimentally by van der Maarel *et al.* [10], for more dilute TMA DNA solutions. In the present study on sodium DNA, due to the relative values of the scattering length densities, the counterions are virtually invisible and, hence, the DNA structure is observed.

Durand *et al.* [5], performed SAXS experiments on solutions of DNA fragments in the cholesteric and hexagonal phases. For the cholesteric phase, they observed a scattering pattern with a strong circular maximum. Robinson *et al.* [11], have observed a similar peak with concentrated solutions of PBLG and proposed a local hexagonal order perpendicular to the molecular axis for the cholesteric phase. Nematic phases of magnetically oriented rod-like polymers such as TMV virus and PBLG have been studied by Meyer and coworkers [12, 13]. In the present SANS study, similar scattering patterns are presented, but additional information can be obtained due to the macroscopic alignment of the samples. For SANS on micellar solutions, this alignment was effected by, for example, a shear gradient [14, 15] or a magnetic field [16, 17]. Here, for the cholesteric solutions of DNA fragments, an external magnetic field was applied during the experiments. DNA fragments [18] tend to align perpendicular to an applied external magnetic field, and in liquid crystalline solutions, this results in an orientation of the (rotating) director perpendicular to this field [6].

If the magnetic field is parallel to the incoming neutron beam ($B_{\parallel}$ configuration, see figure 1) the small angle scattering is isotropic due to the helical distribution in director orientation parallel to the detector. In the other configuration, in which the magnetic field is perpendicular to the incoming beam ($B_{\perp}$ configuration, see figure 2), the director plane is perpendicular to the detector. Now, the scattering is anisotropic due to the fact that the distribution in director orientation with respect to the momentum transfer vector varies with the direction of momentum transfer.

The change in intermolecular structure through the phase transition from the isotropic to the cholesteric phase is of interest here. Unfortunately, there is no theoretical expression for this intermolecular structure available. However, the intramolecular contribution to the scattering pattern provides information about the degree of ordering of the liquid crystalline solutions. In fact, the orientation distribution of the DNA fragments can be obtained by comparing the experimental data to the form function of a uniform rod, including a gaussian distribution in the direction of the DNA molecules with respect to the director plane with a characteristic distribution width.

2. Theory

The coherent part of the solvent subtracted intensity of neutron radiation scattered by a DNA solution without added simple salt reads [19]

$$I(\mathbf{q}) = c[\bar{b}_{\mathrm{m}}^2 S_{\mathrm{mm}}(\mathbf{q}) + 2\bar{b}_{\mathrm{m}}\bar{b}_{\mathrm{c}} S_{\mathrm{mc}}(\mathbf{q}) + \bar{b}_{\mathrm{c}}^2 S_{\mathrm{cc}}(\mathbf{q})] \tag{1}$$

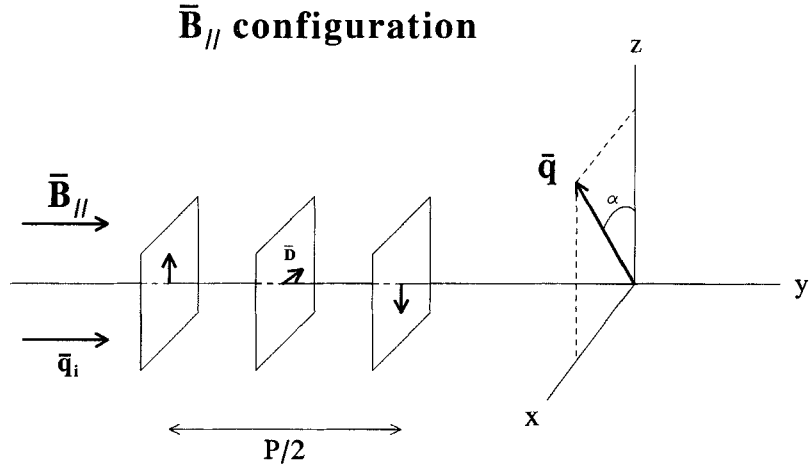

Figure 1. Definition of the various vectors and axes for the $B_{\|}$ configuration. $B_{\|}$ and $\mathbf{q}_i$ represent the direction of the external magnetic field and the incoming neutron beam, respectively. The average direction of the DNA molecules is perpendicular to the external magnetic field. The vector **D** denotes the director, which rotates in the director plane about the cholesteric axis. The characteristic pitch is denoted by P. The momentum transfer vector is represented by **q**, situated in the two-dimensional detector plane (i.e. xz-plane). The horizontal of the detector is along the z axis.

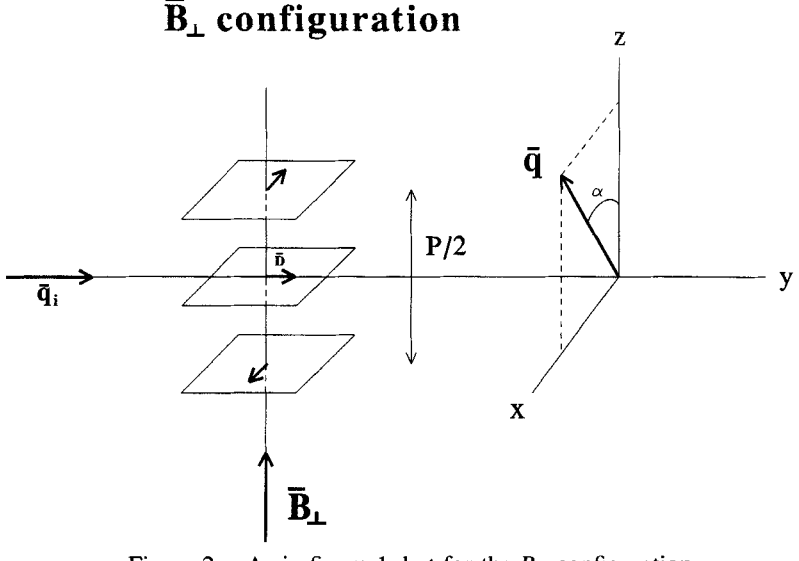

Figure 2. As in figure 1, but for the $B_{\perp}$ configuration.

with c the concentration in number of monomer nucleotides per unit volume. The monomer–monomer, monomer–counterion and counterion–counterion partial structure function are denoted by S_{mm}, S_{mc} and S_{cc}, respectively. The nucleotide scattering length contrast $\bar{b}_m$ has been calculated using the values reported by Jacrot [20] and according to the base composition A:G:C:T:5-methyl-cytosine = 0·28:0·22:0·21:0·28:0·01 [21]. In pure water, this scattering length contrast takes the value $11{\cdot}38 \times 10^{-12}$ cm, whereas the corresponding value of the

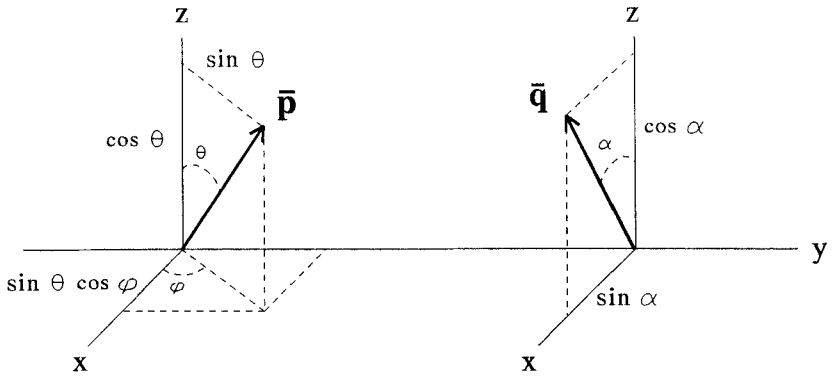

Figure 3. Definition of the various angles concerning the direction of the DNA helix axis (**p**) and the momentum transfer vector (**q**). With these definitions, the orientation parameter μ reads: $\mu = \mathbf{p} \cdot \mathbf{q} = \sin(\alpha)\sin(\theta)\cos(\varphi) + \cos(\alpha)\cos(\theta)$.

sodium counterion $\bar{b}_c$ equals $-0{\cdot}11 \times 10^{-12}$ cm. Accordingly, the condition $|\bar{b}_m| \gg |\bar{b}_c|$ is fulfilled and the scattered intensity is dominated by the DNA structure

$$I(\mathbf{q}) = c\bar{b}_m^2 S_{mm}(\mathbf{q}). \tag{2}$$

Neglect any correlation between molecular structure and intermolecular interaction, the DNA structure function can be expressed as a sum of the form function $F(\mathbf{q})$ and an intermolecular interference contribution $S^{inter}(\mathbf{q})$

$$S_{mm}(\mathbf{q}) = F(\mathbf{q}) + S^{inter}(\mathbf{q}). \tag{3}$$

For sufficiently high values of momentum transfer, the intermolecular interference contribution can be neglected and, hence, in this **q**-range, the scattered intensity is directly proportional to the form function

$$I(\mathbf{q}) = c\bar{b}_m^2 F(\mathbf{q}). \tag{4}$$

The form function is a monotonic decreasing function of **q**. Due to the intermolecular interference contribution $S^{inter}(\mathbf{q})$, a maximum occurs in the total structure function (equation (3)) and, hence, in the scattering pattern. The high **q** part of the scattering range is of particular interest, because in the absence or neglect of intermolecular interference, the data can be compared with the theoretical form function of a rod. The DNA fragment is assumed to be a uniform rod with length L and radius r_p. For a certain orientation of the DNA fragment with respect to the momentum vector **q**, the form function reads

$$F(q,\mu) = N_m\left[\frac{\sin(q\mu L/2)2J_1(qr_p\sqrt{(1-\mu^2)})}{(q\mu L/2)(qr_p\sqrt{(1-\mu^2)})}\right]^2. \tag{5}$$

Here N_m is the number of monomers per fragment and $q = |\mathbf{q}|$. J_1 denotes the first order Bessel function of the first kind. The fragment orientation is given by the inproduct $\mu = \mathbf{p} \cdot \mathbf{q}$, **p** being the unit vector of the z axis of the polymer helix (see figure 3).

Finally, an orientation averaging has to be performed. For this purpose the magnetic field induced liquid crystalline orientational order has to be evaluated. First, the

anisotropic scattering in the $B_\perp$ configuration will be evaluated. As will be shown below, the scattering in the $B_\parallel$ configuration follows immediately as a special case of the former situation.

As displayed in figure 2, in the $B_\perp$ configuration, the director plane is parallel to the xy-plane, whereas the detector is in the xz-plane. the various angles are defined in figure 3. The orientation of the momentum vector with respect to the horizontal in the detector plane (defined as being the z axis in figures 1 and 2) is characterized by the angle α. For an individual fragment, the projected orientation within the director plane is described by the angle φ, whereas the polar angle $(\theta - \pi/2)$ gives the tilt away from this plane. With these definitions, the orientation parameter μ can be rewritten

$$\mu = \sin(\alpha)\sin(\theta)\cos(\varphi) + \cos(\alpha)\cos(\theta). \tag{6}$$

The orientation averaging of the form function can be performed by using a probability distribution function $P(\theta, \varphi)$. The distribution in angle φ is isotropic due to the helical distribution in director orientation over the sample. The distribution in θ is peaked around $\theta = \pi/2$, because of the magnetic field induced alignment. The distribution in θ is assumed to be Gaussian, i.e.

$$P(\theta, \varphi) = \frac{1}{2\pi}P(\theta) = \frac{1}{2\pi}\exp\left(-\left(\theta - \frac{\pi}{2}\right)^2 \Big/ 2\sigma^2\right), \tag{7}$$

with σ being the standard deviation. The orientation averaged form function reads

$$F(\mathbf{q}) = F(q, \alpha) = \frac{1}{2\pi}\int_0^{2\pi} d\varphi \int_0^{\pi} d\theta \sin(\theta) P(\theta) F(q, \mu) \Big/ \int_0^{\pi} d\theta \sin(\theta) P(\theta). \tag{8}$$

The integrations are numerically performed using a recursive adaptive Newton Cotes 8 panel rule [22].

As can be observed in figure 2, for $\alpha = \pi/2$, the **q**-vector lies within the director plane. This is exactly the same situation as in the case of the $B_\parallel$ configuration (see figure 1), but for any value of α. Accordingly, the isotropic scattering intensity for any value of **q** in the $B_\parallel$ configuration follows immediately from equation (8) with $\alpha = \pi/2$.

3. Experimental

DNA fragments were obtained by a micrococcal nuclease digestion of calf thymus nucleosomal DNA, following the procedure described by Wang *et al.* [23]. After precipitation in cold 2-propanol, the DNA pellet was dried under reduced pressure at room temperature. The DNA was brought to the salt free sodium form by dissolving it in a 50 mM NaCl, 24 mM EDTA buffer (at a DNA concentration of 23 mM nucleotides l^{-1}) and extensive dialysis against pure water. To avoid denaturation, care was taken that the DNA concentration did not reach values below 3 mM nucleotides l^{-1}. Water was deionized and filtered by a Millipore water purification system (Millipore Co.) and its conductivity did not exceed $1 \times 10^{-6}\,\Omega^{-1}\,cm^{-1}$. The final product was freeze dried and stored at 255 K.

To determine the DNA fragment molecular weight distribution, gel permeation chromatography was performed [24]. Some low molecular weight material was present, but at least 75 per cent of the DNA had a $\bar{M}_w/\bar{M}_n$ ratio smaller than 1·1 and was characterized by a $\bar{M}_w$ of 108 000 (163 base pairs). The ratio of the optical absorbances A_{260}/A_{280} was 1·85, indicating that the material is essentially free of protein.

Samples were prepared by dissolving sodium DNA in water without adding low molecular weight salt. Quartz cells with 0·2 cm path length were used. Concentrations

were determined after the experiments by UV absorption measurements at 260 nm, using an extinction coefficient of $20\,mg^{-1}\,ml\,cm^{-1}$.

Three samples were prepared. Sample 2 ($240\,mg\,ml^{-1}$, i.e. $0{\cdot}72\,M$ nucleotides l^{-1}) and sample 3 ($285\,mg\,ml^{-1}$, i.e. $0{\cdot}86\,M$ nucleotides l^{-1}) were fully liquid crystalline. Sample 1 showed phase separation into a transparent isotropic solution and a more dense, birefringent liquid crystal. In the latter part of the solution, the concentration was determined to be $190\,mg\,ml^{-1}$ (i.e. $0{\cdot}57\,M$ nucleotides l^{-1}). In the scattering experiments the neutron beam was focused on the liquid crystalline part of the solution.

Neutron scattering experiments were performed using the LOQ small angle scattering instrument, situated on the pulsed spallation neutron source of the ISIS facility, Rutherford Appleton Laboratory, Didcot, UK. The incident wave length is 2–10 Å at a pulse rate of 25 Hz. The scattered radiation was detected using an effectively 64 cm diameter two-dimensional detector (64×64 pixels) at 4·4 m from the sample position, allowing a momentum transfer range from 0·006 to $0{\cdot}22\,Å^{-1}$. Two sets of experiments were performed with a magnetic field applied subsequently parallel and perpendicular to the incoming neutron beam. In the former configuration, the field strength was 0·5 T and in the latter 0·8 T. The temperature at the sample position was controlled at 298 K, using a water thermostat.

The counting time per sample, i.e. solution or solvent, was approximately 4 h. Data correction allowed for the sample transmission, the detector efficiency and the incident neutron spectrum shape. Absolute scattering intensities were obtained by reference to the coherent scattering from a partially deuteriated polystyrene sample. The scattering of the solvent (i.e. pure water) was subtracted and no incoherent correction has been performed.

4. Results and discussion

Neutron scattering experiments were performed with the magnetic field aligned both parallel ($B_\parallel$) and perpendicular ($B_\perp$) to the incoming neutron beam. Figure 4 displays a contour plot of the two dimensional scattering intensity of sample 2 in the $B_\parallel$ configuration. The scattering pattern is isotropic due to the helical distribution in director orientation within the director plane parallel to the detector (see figure 1). Figure 5 shows the corresponding intensity for the $B_\perp$ configuration. Now the intensity shows anisotropic behaviour, because of the fact that the distribution in director orientation with respect to the momentum transfer vector varies with the direction of momentum transfer, i.e. the angle α (see figure 2). The other samples show similar behaviour. The right side of all scattering patterns is slightly more intense than the left side. This is due to a technical artefact.

In the anisotropic case, the intensity shows maxima for $\alpha = 0$ and $\alpha = \pi$. The isotropic scattering in the $B_\parallel$ configuration and the anisotropic scattering in the $B_\perp$ configuration agree with the cholesteric structure of the solutions, as has been described in the introduction. In both magnetic field configurations, the scattering pattern shows a circular maximum. This indicates that the characteristic intermolecular structure within the director plane is similar to the corresponding structure perpendicular to this plane. The scattering ring moves to higher **q**-values as the concentration increases. This shift indicates a decrease of the distance scale between DNA fragments with increasing concentration. Both the anisotropic scattering in the $B_\perp$ configuration, as well as the isotropic scattering in the $B_\parallel$ configuration, will be detailed below separately.

Our anisotropic scattering patterns differ from those observed for other systems. Meyer and coworkers studied the X-ray scattering of magnetically oriented nematic

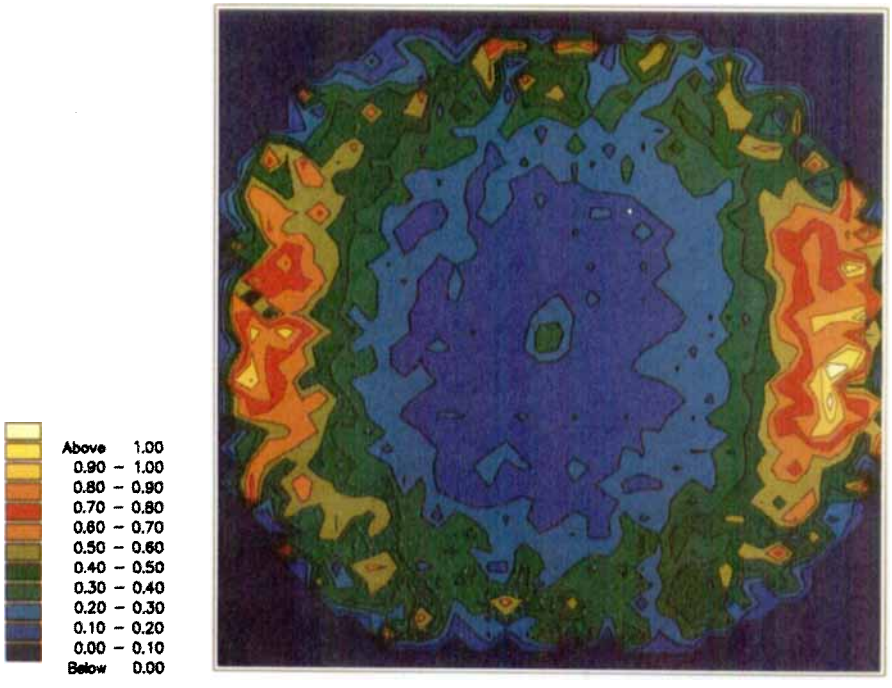

Figure 4 Contour plot of the two-dimensional scattering intensity of sample 2 in the $B_{\parallel}$ configuration. The scattering pattern is isotropic due to the helical distribution in director orientation within the director plane parallel to the detector.

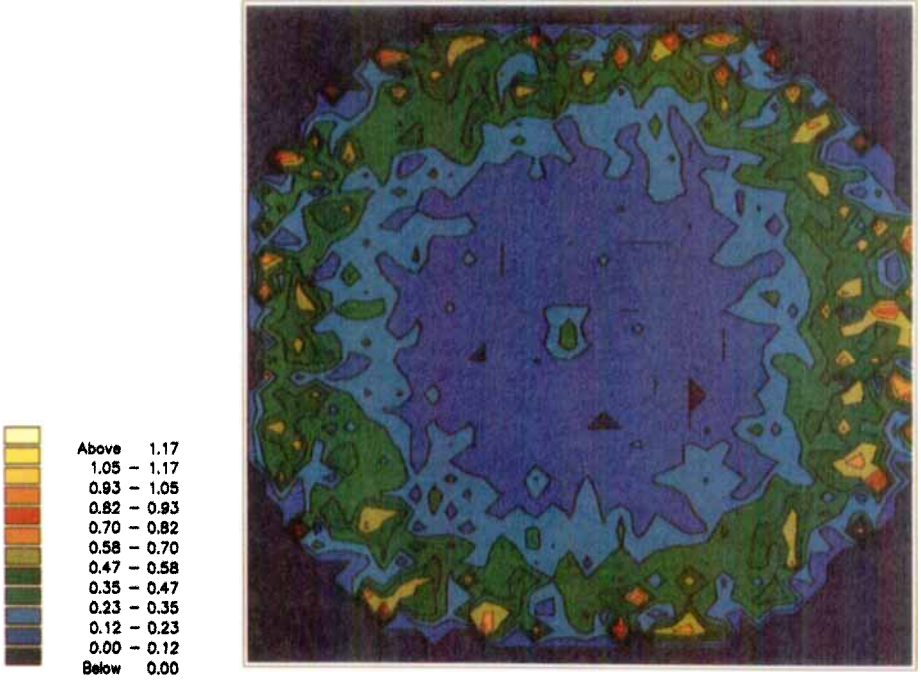

Figure 5. Contour plot of the two dimensional scattering intensity of sample 2 in the $B_{\perp}$ configuration. The scattering pattern is anisotropic due to the fact that the distribution in director orientation with respect to the momentum transfer vector varies with the direction of momentum transfer.

phases of PBLG and TMV [12, 13]. They observed a bow-tie like diffraction pattern indicating the considerable difference in the lateral and longitudinal packing of the chains in the nematic phase. Holmes *et al.*, studied the anisotropic scattering of a magnetically oriented lamellar ionic surfactant system [17]. Here the anisotropy in the scattered intensity is more pronounced compared to our results and, moreover, a deviation from circular symmetry was observed. This deviation was interpreted in terms of a difference in intra- and inter-lamellar distances.

First, the results obtained in the $B_{\|}$ configuration will be discussed. In this case the average orientation of the DNA fragments is parallel to the detector plane

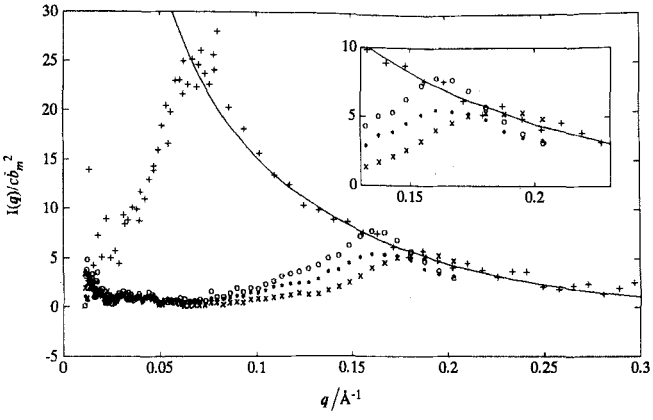

Figure 6. The angular averaged scattering intensities divided by the constant $c\bar{b}_m^2$ in the $B_{\|}$ configuration (○) 190 mg ml^{-1}; (*) 240 mg ml^{-1}; (×) 285 mg ml^{-1}). For comparison the DNA structure function of a diluted isotropic TMA DNA solution has also been included: (+) 35 mg ml^{-1}. The solid line represents the isotropic orientation average of the form function of a rod with $L = 500$ Å and $r_p = 8$ Å. The inset shows a magnification of the high **q** region.

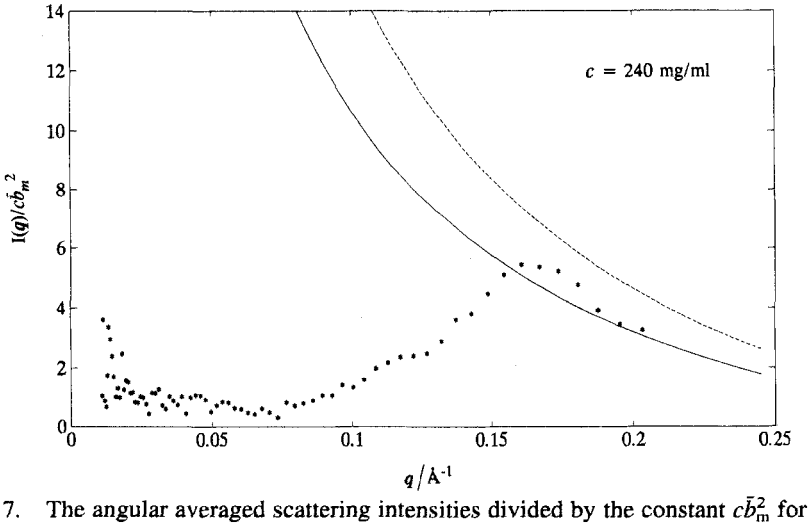

Figure 7. The angular averaged scattering intensities divided by the constant $c\bar{b}_m^2$ for sample 2 in the $B_{\|}$ configuration. The dashed line represents the isotropic orientation average of the form function and the solid line an average with $\alpha = \pi/2$ and $\sigma = 21°$.

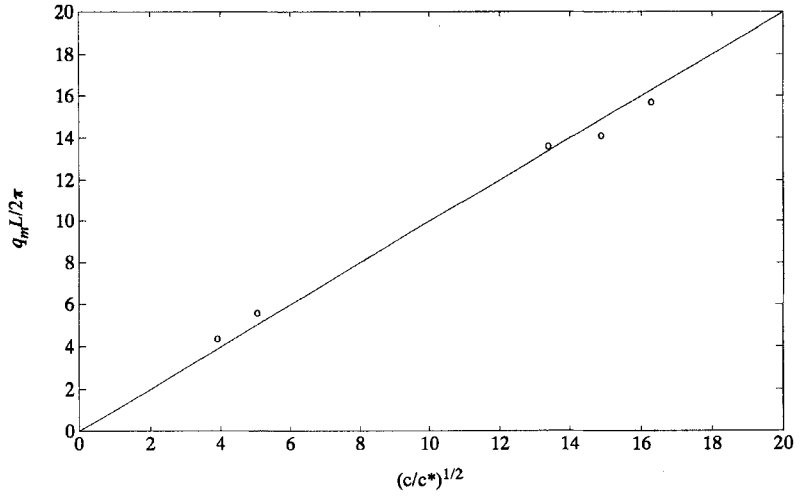

Figure 8. The dimensionless ratio $\mathbf{q}_m L/2\pi$ versus $(c/c^*)^{1/2}$ for two diluted, isotropic samples (17 and 35 mg ml^{-1}) and the present liquid crystalline samples (190, 240 and 285 mg ml^{-1}). The slope of the best fitting solid line is 1·03.

(see figure 1) and, hence, the scattering is isotropic. Figure 6 shows the angular averaged scattering intensities divided by the constant $c\bar{b}_m^2$ of all three samples. The data represent the partial structure function $S_{mm}(\mathbf{q})$ versus $\mathbf{q}$, provided that the incoherent scattering contribution can be neglected. The DNA structure function obtained on a more diluted, isotropic TMA DNA solution of 35 mg ml^{-1} (i.e. below the phase transition; data obtained at the Institute Laue-Langevin) [10] is included too. For relatively high values of momentum, transfer ($\mathbf{q} \geqslant 0{\cdot}18$ Å^{-1}), all experimental structure functions tend to coincide. This indicates that for those values of $\mathbf{q}$, intermolecular interference effects are small and the structure functions more or less represent the form function $F(\mathbf{q})$.

In figure 6 the solid line represents the isotropic orientation average of the rod form function (equation (5); $L = 500$ Å, $r_p = 8$ Å). As one can see in the inset of figure 6, at the high $\mathbf{q}$ end, this curve coincides rather well with the data obtained on the dilute, isotropic sample. However, the data obtained on the liquid crystalline samples 1 and 2 tend to take somewhat smaller values at high $\mathbf{q}$. This could not be confirmed by the more concentrated sample 3, due to the fact that here no clear maximum is observed (limited $\mathbf{q}$-range). This behaviour can be explained by the fact that in the liquid crystalline samples, the form function depends on the orientation distribution of the DNA fragments, even in the situation in which the two-dimensional scattering pattern is isotropic. Another explanation is the presence of residual intermolecular effects at and beyond the peak maximum.

As has been pointed out in the theoretical section, the form function can be evaluated by introducing a gaussian distribution in θ with a characteristic standard deviation σ, with $(\theta - \pi/2)$ being the angle between a certain DNA fragment and the director plane. Figure 7 shows the data of sample 2 in the $B_\parallel$ configuration and includes, apart from an isotropic orientation average of the form function, an average with $\alpha = \pi/2$ and $\sigma = 21°$ (equation (8)). The latter curve coincides with the experimental data for high $\mathbf{q}$-values, whereas the former one is clearly too intense. Moreover, the data indicate the presence of residual intermolecular effects at the peak maximum. If a very broad distribution is chosen, equation (8) (with $\alpha = \pi/2$) reduces to the isotropic orientation

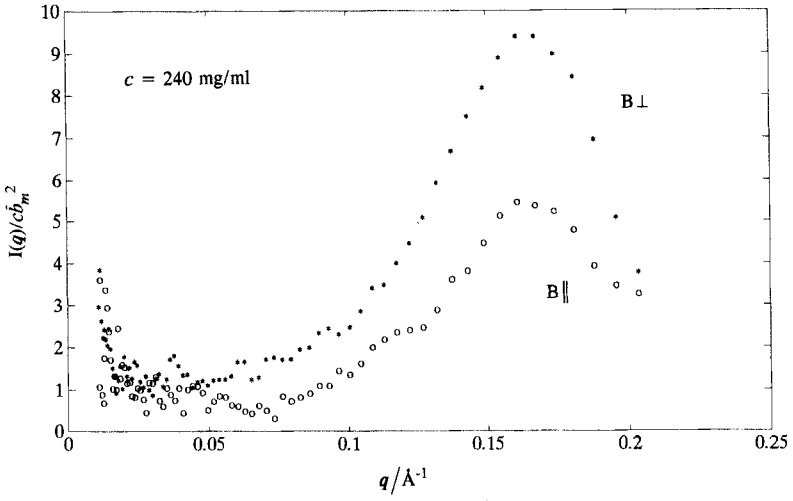

Figure 9. The angular averaged scattering intensities divided by the constant $c\bar{b}_m^2$ for sample 2 in the $B_\parallel$ configuration (○) and the $B_\perp$ configuration (*).

average of the form function. The value for σ used here was estimated from the anisotropic scattering data in the $B_\perp$ configuration (see below). In the $B_\parallel$ configuration, the dependence of the theoretical form function on σ is not sufficiently pronounced to allow for an accurate estimation of σ.

The maximum at momentum transfer $\mathbf{q}_m$ occurs due to the onset of interference effects and is indicative of a solution structure. In both the $B_\parallel$ and the $B_\perp$ configuration, the scattering pattern is circular. Furthermore, in both configurations, the maximum occurs at the same value of momentum transfer $\mathbf{q}_m$, as will be shown below. This indicates an isotropic intermolecular local structure with respect to the director. Since at higher concentrations, interference effects become important on a shorter length scale, the peak position shifts to higher $\mathbf{q}$-values with increasing concentration. Above the overlap concentration $C^* = 1/L^3$, this peak scales as $c^{1/2}$ both for flexible synthetic polyelectrolytes [25, 26] as well as rod-like biopolymers [27, 28] (below the phase transition). Wang and Bloomfield [27] studied the $\mathbf{q}_m \sim c^{1/2}$ behaviour by small angle X-ray scattering on isotropic solutions of 160 basepair DNA fragments in the concentration range 30 to 182 mg ml^{-1}. Figure 8 displays the dimensionless ratio $\mathbf{q}_m L/2\pi$ versus $(c/c^*)^{1/2}$ for the present SANS results, as well as for two more diluted isotropic samples, i.e. at a concentration of 17 mg ml^{-1} (neutron scattering results, data obtained at CEN, Saclay; Groot *et al.*, to be published) and 35 mg ml [10]. In the latter two isotropic samples, the counterion of the DNA fragments was tetramethylammonium instead of sodium, which was used in the present study. With no clear discontinuity, the $\mathbf{q}_m \sim c^{1/2}$ behaviour persists up to well within the liquid crystalline regime. Accordingly, throughout the phase transition, there is no apparent change in positional correlation among DNA fragments. At higher concentrations, the cholesteric pitch unwinds and, eventually, a macroscopic hexagonal phase is formed [5]. For our cholesteric solutions, a local hexagonal structure may already exist, although this cannot be directly inferred from the present data. The $\mathbf{q}_m \sim c^{1/2}$ behaviour is in agreement with the intermolecular distances based on a locally hexagonal structure of parallel rods. Provided the maximum corresponds to the Bragg condition, $\mathbf{q}_m = 2\pi/d$, d being the characteristic distance between rods, the scaling takes the form $\mathbf{q}_m L = 2\pi(c/c^*)^{1/2}$. As

is shown in figure 8, this theoretical behaviour reasonably agrees with the experimental results, both in the isotropic as well as the anisotropic solutions.

As displayed in figure 6, only one scattering peak is observed. Unfortunately, the momentum transfer does not extend to sufficiently high values to check any multiple interferences. However, for the DNA cholesteric phase, Durand *et al.* observed only one solution structure X-ray diffraction peak [5]. Accordingly, the absence of multiple peaks is no indication of the absence of an anisotropic solution structure, as was suggested before [27]. The shape of the diffraction peaks is similar to the situation in more diluted, isotropic solutions. This indicates that the liquid crystal displays liquid-like positional order.

Now, the anisotropic scattering in the $B_\perp$ configuration will be discussed. As has been pointed out before, in both the $B_\parallel$ and the $B_\perp$ configuration, the scattering patterns of all samples are circular (see figures 4 and 5) and the data can be angularly averaged. Figure 9 shows the angular averaged scattering intensities of sample 2 divided by the constant $c\bar{b}_m^2$ in both configurations. In both situations the shape and the peak position of the curves are similar, but the intensity in the $B_\perp$ configuration is more or less twice as high as in the isotropic configuration. The other samples show similar behaviour. This increase in intensity is due to magnetic field induced alignment effects and will be interpreted in terms of a preferential orientation averaged form function.

Now, the α-dependence of the structure function at a certain value of $\mathbf{q}$ will be discussed,, α being the angle between $\mathbf{q}$ and the horizontal of the detector (defined) by the z axis in figure 3). The value of the structure function versus α for a high value of $\mathbf{q}$ on the right hand side of the peak ($\mathbf{q} \approx 1{\cdot}1\ \mathbf{q}_m$) has been collected for both

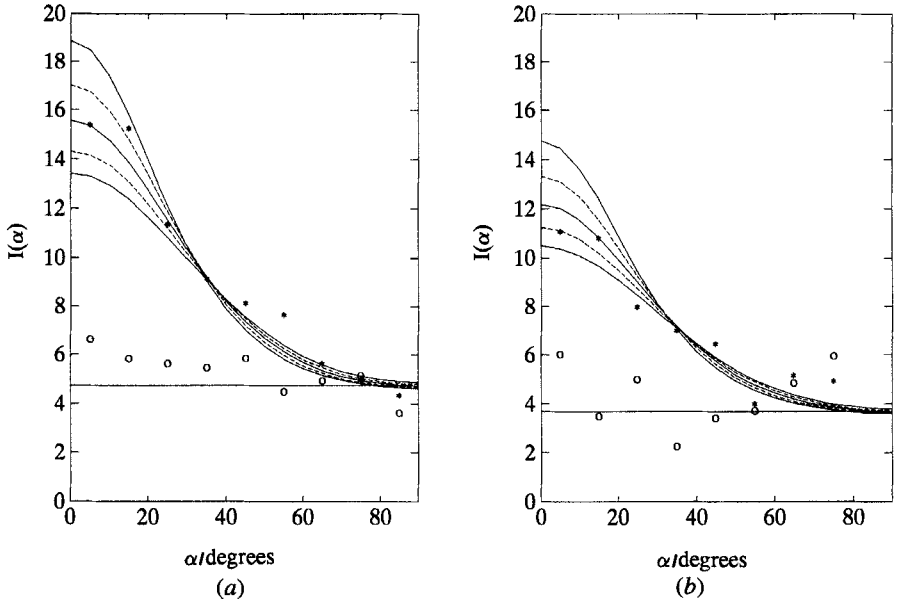

Figure 10. (*a*) The α-dependence of the scattering at $\mathbf{q}_m$ of sample 2 in the $B_\parallel$ configuration (○) and the $B_\perp$ configuration (*). The straight horizontal line represents the value of the theoretical form function for the $B_\parallel$ configuration. The other five lines refer to theoretical curves with $\sigma = 17°$, 19°, 21°, 23° and 25° from top to bottom. (*b*) As in (*a*), but at $\mathbf{q} = 1{\cdot}1\ \mathbf{q}_m$.

Optimized values for σ at $\mathbf{q}_m$ and $1{\cdot}1\,\mathbf{q}_m$.

DNA concentration/mg ml^{-1}	σ at $\mathbf{q}_m$	σ at $1{\cdot}1\,\mathbf{q}_m$
190	20°	22°
240	21°	20°
285	18°	18°

configurations. Therefore the scattering intensities were rebinned into angular segments of 10 degrees. As has been shown in the $B_\parallel$ case, for $\mathbf{q} \geq 0{\cdot}18$ Å^{-1}, intermolecular interference effects are small and/or negligible. Beyond the peak maximum, however, the signal also decreases with increasing value of $\mathbf{q}$. Therefore, the α-dependent data at $\mathbf{q}_m$ have been collected too. As will be shown below, the presence of interference effects at $\mathbf{q}_m$ does not significantly influence the derived distribution width.

Figure 10 displays the α-dependence of the scattering at $\mathbf{q}_m$ (see figure 10(*a*)) and at $\mathbf{q} \approx 1 \cdot 1\,\mathbf{q}_m$ (figure 10(*b*)) of sample 2 in both configurations. The results obtained on the four different detector quadrants have been averaged. As expected, the data show no significant α-dependence in the $B_\parallel$ configuration. As has been pointed out in the theoretical section, the form function can be evaluated by introducing a gaussian distribution in θ with a characteristic σ, $(\theta - \pi/2)$ being the angle between a certain DNA fragment and the director plane. The scattering data can be compared with theoretical values of the form function with different values of σ. Figures 10(*a*) and (*b*) include theoretical curves with $\sigma = 17°$, 19°, 21°, 23° and 25° from top to bottom. It is clear that the theoretical curves are quite sensitive to the value of σ in the anisotropic situation. Here, the value of σ can be estimated with an accuracy of the order of 10 per cent. The value of the theoretical form function for the $B_\parallel$ configuration (i.e. the value at $\alpha = \pi/2$ in the $B_\perp$ configuration) has also been included in figure 10. In the range, say, $\alpha > 60°$, the intensities obtained in both magnetic field configurations coincide, in agreement with the theoretical behaviour of the form function.

The table shows the optimized values for σ for all samples at both $\mathbf{q}$-values. Within experimental error, the derived values for σ are the same for $\mathbf{q} = \mathbf{q}_m$ and $\mathbf{q} = 1{\cdot}1\mathbf{q}_m$. Accordingly, any residual intermolecular contribution probably has a negligible effect on the value of σ. The width of the orientation distribution is of the order of 20° and seems to decrease slightly with increasing concentration. The value of σ is possibly related to the twisting effect induced by the electrostatic interaction between DNA fragments [29]. This twisting conflicts with the limited volume available to accommodate the polyions and, hence, a competition occurs. The concentration effect is presumably due to the progressively restricted available volume.

The present experiments were performed using the highest available magnetic field strengths ($B_\parallel = 0{\cdot}5$ T, $B_\perp = 0{\cdot}8$ T). Since in the $B_\parallel$ configuration, the dependence of the theoretical form function on σ is not sufficiently pronounced to make an accurate estimation of σ, no conclusions can be drawn regarding any possible magnetic field strength dependence. To investigate a possible dependence of the distribution width, a ^{23}Na counterion NMR study was performed. The sodium resonance shows a quadrupole splitting which is indicative of the degree of ordering. In the range 2·1 to 6·3 T, this splitting was constant. However, if the field strength is reduced to 0·6 T, the splitting decreases about 10 per cent. This indicates a possible magnetic field strength effect on the value of σ, but, since the direct relation between the line splittings and

the ordering of the DNA fragments is not known, from these experiments the magnitude of this effect cannot be estimated.

5. Conclusions

The isotropic scattering pattern in the $B_{\parallel}$ configuration and the anisotropic scattering in the $B_{\perp}$ situation agree with the cholesteric structure of the liquid crystalline solutions. The local positional solution structure probed by SANS appears to be similar to that in isotropic solutions. The peak positions scale with $c^{1/2}$, which can be interpreted using a locally hexagonal structure. However, the absence of multiple interferences indicates liquid-like positional order. The circular scattering patterns indicate that the characteristic distance between DNA molecules within the director plane is similar to that in the direction perpendicular to this plane. Since the helical pitch is of the order of 2 μm, the director tilts less than 1° over the characteristic distance d between rods. In this perspective, these liquid crystalline solutions can be considered nematic on a local distance scale.

The isotropic scattering in the $B_{\parallel}$ configuration is not very suitable for studying the orientation distribution of the liquid crystalline solutions. It can be concluded, though, that the mean orientation of the DNA molecules is perpendicular to the external magnetic field. The anisotropic scattering pattern in the $B_{\perp}$ configuration shows the degree of orientation ordering, i.e. the distribution of the DNA fragments with respect to the director plane. The angular averaged scattering can be interpreted in terms of a rod form function including a distribution of the orientation of the DNA molecule with respect to the director plane. The assumption has been made that this distribution is gaussian.

The standard deviation of this distribution is about 20° for all concentrations investigated here. There seems to be a very slight decrease of σ with increasing concentration. Regarding an estimated error of about 10 per cent, no firm conclusions can be drawn from this concentration dependence. Besides a tilt of the fragments out of the director plane, this distribution can also refer to a macroscopic distribution in the orientation of the cholesteric axis. From the present data this effect cannot be estimated and future experiments are called for to investigate the effects of magnetic field strength. The distribution width most likely results from a competition of the twisting effect favouring perpendicular orientation of two interacting rod-like polyelectrolytes and the limited available free volume to accommodate the polyions [29]. These experiments do not provide any information regarding the distribution of the projected orientation of the DNA fragment within the director plane, since the macroscopic average is isotropic due to the helical pitch. However, due to the local nematic nature of these systems, the orientation distribution is expected to be symmetric with respect to the director. The corresponding order parameter $S = \langle P_2(\cos\theta)\rangle$ is of the order of 0·85. This value compares favorably to the experimental results obtained on the nematic TMV virus liquid crystals [13] and to the typical theoretical values based on the second virial approximation [29, 30].

The authors would like to acknowledge NWO (Nederlandse organisatie voor Wetenschappelijk Onderzoek) for financial support, the staff of the ISIS facility for technical support and M. Mandel for his continuous interest and valuable discussions.

References

[1] RILL, R. L., STRZELECKA, T. E., DAVIDSON, M. W., and VAN WINKLE, D. H., 1991, *Physica* A, **176,** 87.

[2] GROOT, L. C. A., VAN DER MAAREL, J. R. C., and LEYTE, J. C., 1994, *J. phys. Chem.*, **98,** 2699.

[3] LIVOLANT, F., 1987, *J. Phys., France,* **48,** 1051.

[4] LIVOLANT, F., LEVELUT, A. M., and BENOIT, J. P., 1989, *Nature, Lond.,* **339,** 724.

[5] DURAND, D., DOUCET, J., and LIVOLANT, F., 1992, *J. Phys. II, France,* **2,** 1769.

[6] BRANDES, R., and KEARNS, D., 1986, *Biochemistry,* 5890.

[7] VAN WINKLE, D. H., DAVIDSON, M. W., CHEN, W. X., and RILL, R. L., 1990, *Macromolecules,* **23,** 4140.

[8] STRZELECKA, T. E., and RILL, R. L., 1992, *J. phys. Chem.,* **96,** 7796.

[9] BRANDES, R., and KEARNS, D. R., 1988, *J. phys. Chem.*, **92,** 6836.

[10] VAN DER MAAREL, J. R. C., GROOT, L. C. A., MANDEL, M., JESSE, M., JANNINK, G., and RODRIGUEZ, V., 1992, *J. Phys. II, France,* **2,** 109.

[11] ROBINSON, C., WARD, J. C., and BEEVERS, R. B., 1958, *Discuss. Faraday Soc.,* **25,** 29.

[12] AO, X., WEN, X., and MEYER, R. B., 1991, *Physica* A, **176,** 63.

[13] OLDENBOURG, R., WEN, X., MEYER, R. B., and CASPAR, D. L. D., 1988, *Phys. Rev. Lett.,* **61,** 1851.

[14] HAYTER, J. B., and PENFOLD, J., 1984, *J. phys. Chem.,* **88,** 4589

[15] KALUS, J., and HOFFMAN, H., 1987, *J. chem. Phys.,* **87,** 714.

[16] HERBST, L., HOFFMAN, H., KALUS, J., REIZLEIN, K., SCHMELZER, U., and IBEL, K., 1985, *Ber. Bunsenges. phys. Chem.,* **89,** 1050.

[17] HOLMES, M. C., SMITH, A. M., and LEAVER, M. S., 1993, *J. Phys. II, France,* **3,** 1357.

[18] MARET, G., v. SCHICKFUS, M., MAYER, A., and DRANSFELD, K., 1975, *Phys. Rev. Lett.,* **35,** 397.

[19] JANNINK, G., and VAN DER MAAREL, J. R. C., 1991, *Biophys. Chem.,* **41,** 15.

[20] JACROT, B., 1976, *Rep. Prog. Phys.,* **39,** 911.

[21] MAHLER, H. R., and CORDES, E. H., 1971, *Biological Chemistry,* second edition (Harper & Row), Chap. 5.

[22] *Matlab Numeric Computation Software,* 1991 (The Math Works Inc.).

[23] WANG, L., FERRARI, M., and BLOOMFIELD, V. A., 1990, *BioTechniques,* **9,** 24.

[24] NICOLAI, T., VAN DIJK, L., VAN DIJK, J. A. P. P., and SMIT, J. A. M., 1987, *J. Chrom.,* **389,** 286.

[25] NIERLICH, M., WILLIAMS, C. E., BOUÉ, F., COTTON, J. P., DAOUD, M., FARNOUX, B., JANNINK, G., PICOT, C., MOAN, M., WOLFF, C., RINAUDO, M., and DE GENNES, P. G., 1979, *J. Phys., France,* **40,** 701.

[26] KAJI, K., URAKAWA, H., KANAYA, T., and KITAMURA, R., 1988, *J. Phys., France,* **49,** 993.

[27] WANG, L., and BLOOMFIELD, V. A., 1991, *Macromolecules,* **24,** 5791.

[28] MAIER, E. E., KRAUSE, R., DEGGELMANN, M., HAGENBÜCHLE, M., WEBER, R., and FRADEN, S., 1992, *Macromolecules,* **25,** 1125.

[29] STROOBANTS, A., LEKKERKERKER, H. N. W., and ODIJK, TH., 1986, *Macromolecules,* **19,** 2232.

[30] KHOKLOV, A. R., 1991, *Liquid Crystallinity in Polymers: Principles and Fundamental Properties,* edited by A. Ciferri (VCH Publishers Inc.), Chap. 3.